Available online at www.sciencedirect.com
ScienceDirect
Ceramics International 37 (2011) 119–125
CERAMICS INTERNATIONAL
www.elsevier.com/locate/ceramint

Fabrication, microstructure and optical properties of polycrystalline Er^{3+}:$Y_3Al_5O_{12}$ ceramics

Jun Zhou [a,b], Wenxin Zhang [a,b], Liang Wang [a,b], Yiqiang Shen [a,b], Jiang Li [a], Wenbin Liu [a], Benxue Jiang [a], Huamin Kou [a], Yun Shi [a], Yubai Pan [a,*]

[a] Key Laboratory of Transparent and Opto-functional Advanced Inorganic Materials, Shanghai Institute of Ceramics, Chinese Academy of Sciences, 1295 Ding Xi Road, Shanghai 200050, China
[b] Graduate School of the Chinese Academy of Sciences, 19A Yuquan Road, Beijing 100039, China

Received 2 April 2010; received in revised form 28 June 2010; accepted 24 July 2010
Available online 21 August 2010

Abstract

Highly transparent polycrystalline Er^{3+}:$Y_3Al_5O_{12}$ (Er:YAG) ceramics with different Er^{3+} ions content from 1% to 90% were prepared by the solid-state reaction and the vacuum-sintering technique. The grain boundary is clean and narrow with a width of about 1 nm. The best sintering temperature of the ceramics is about 1800 °C. The relationships between fabrication, microstructure and transparency of the ceramics were discussed. Grain size distributions in axial direction of cylinder samples were characterized by electron probe micro-analyzer (EPMA). The luminescence spectra were measured and discussed.

Keywords: C. Optical properties; Fabrication; Microstructure; Er:YAG transparent ceramics

1. Introduction

In recent years, highly transparent polycrystalline rare-earth element doped $Y_3Al_5O_{12}$ (YAG) ceramics (especially Nd:YAG) has become a kind of significant laser substrate material with the assistance of the improved fabrication technologies and the diode laser excitation system. It has been proved that YAG-structure ceramics materials exhibit excellent laser performance similar to YAG single crystals [1–8]. And diode-pumped Nd:YAG, Yb:YAG, composite YAG/Nd:YAG/YAG ceramics laser experiments have also been successfully performed in our group [9–12]. Among the rare-earth doped YAG-structure materials, high content Er^{3+}:$Y_3Al_5O_{12}$ (Er:YAG) single crystal is an important laser material to obtain laser emission at 2.94 μm wavelength, which is widely utilized by the medical community because of the strong absorption by water in this wavelength range [13,14]. It is significant to substrate Er:YAG ceramics for the crystal materials as laser emitting substrate.

The microstructure of Nd:YAG ceramics has been characterized and discussed in some points of view [6,8,15]. If grain sizes were smaller than 2 μm, the microscopic variation of the Nd^{3+} ion concentration, luminescence emission, and index maybe minimized, which could lead to less light scatter at the pump and lasing wavelengths [16]. The factors determining grain sizes could be particle sizes of starting powders, sintering temperature and soaking time. Decreasing soaking time is an effective way to prevent grains growing too large. But there is a natural contradiction between the soaking time and the transparency. To obtain highly transparent YAG ceramics, it requires certain sintering temperature and long enough soaking time.

In this paper, polycrystalline Er:YAG ceramics had been obtained by the solid-state reaction and the vacuum-sintering technique, and the relationships between fabrication, microstructure and transparency of the ceramics were found and discussed.

2. Experimental procedure

The commercial high purity α-Al_2O_3 (>99.99%, $D_{50} \approx 0.38$ μm), Y_2O_3 (>99.99%, $D_{50} \approx 3.35$ μm), and Er_2O_3 (>99.99%, $D_{50} \approx 7.2$ μm) were used as starting

* Corresponding author. Tel.: +86 21 52412820; fax: +86 21 52413903.
E-mail address: ybpan@mail.sic.ac.cn (Y. Pan).

0272-8842/$36.00
doi:10.1016/j.ceramint.2010.08.025

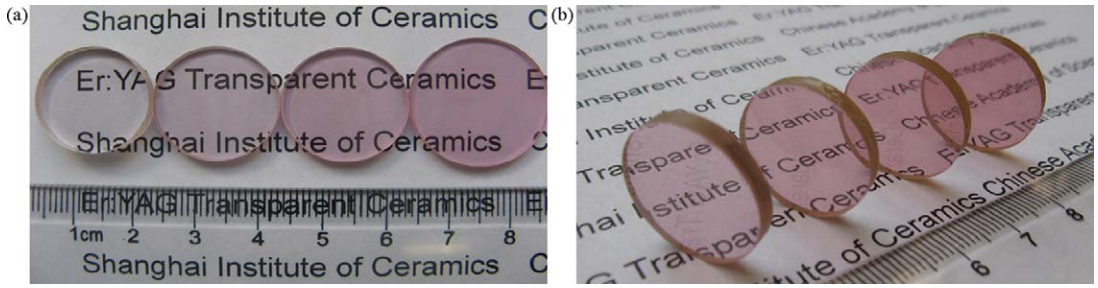

Fig. 1. The mirror-polished Er:YAG ceramics with erbium content from the left to the right: (a) 1, 5, 10, and 15 at.%; (b) 30, 50, 70, and 90 at.%.

materials. These powders were weighed according to the different stoichiometric ratios of the Er:YAG and milled with Al_2O_3 balls for 12 h with ethanol and tetraethyl orthosilicate. After dried and sieved through 200-mesh screen, the powder mixtures were dry-pressed at 3T to form a disk with a diameter of 25 mm and follow-up isostatically cold-pressed at 250 MPa. The powder compacts were vacuum-sintered at 1780 °C for 20 h under 10^{-3} Pa, then annealed at 1450 °C for 20 h under atmosphere.

To characterize the grains of the cross section, 1 at.% Er:YAG cylinder samples were cut in axial direction, then mirror-polished and etched at 1500 °C for 1 h under atmosphere. The microstructures were observed by the electron probe micro-analyzer (EPMA) (Model JSM-6700, JEOL, Tokyo, Japan). Disk specimens machined to disks (Ø20 mm × 2 mm) and mirror-polished on both surfaces were used to measure optical transmittance (Model U-2800 Spectrophotometer, Hitachi, Tokyo, Japan). To measure the fluorescence spectra (Fluorolog-3, Jobin Yvon, Paris, France), the samples were excited with a 980 nm laser diode (LD).

3. Results and discussion

Fig. 1(a) and (b) are photographs of mirror-polished Er:YAG transparent ceramics fabricated through above method with different erbium content from 1% to 90%. Along with increasing erbium content, the specimens look pinker due to the light absorption of Er^{3+} at the visible band. With the beautiful color, the highly transparent pink ceramics can be cut and machined into jewelry because of the crystal-like appearance. Fig. 2(a) is the in-line transmittance spectra of five samples with erbium content of 1%, 30%, 50%, 70%, 90% respectively. It can be seen that Er:YAG ceramics with excellent optical properties have been obtained through the vacuum-sintering preparation. All the main absorption bands of Er^{3+} ions are distinctively strengthened with more erbium added, and that means Er^{3+} ions take the place of Y^{3+} ions successfully owing to the similar chemical properties and ionic radiuses of element Er (1.004 Å) and Y (1.019 Å), which are from the same subgroup – IIIB. And the absorption bands centered at 255, 381, 524, 646, 788, and 966 nm correspond to energy level of $^4D_{7/2}$, $^4G_{11/2}$, $^2H_{11/2}$, $^4F_{9/2}$, $^4I_{9/2}$, and $^4I_{11/2}$ manifold respectively. From Fig. 2(b) we can see that after fully air annealing the transmittance is raised at the visible band. As we all know, vacuum-sintering process could bring in lots of oxygen vacancies. During the air annealing, oxygen atoms can diffuse into the polycrystal structure and decrease the concentration of oxygen vacancies [17]. The F-type centers in the ceramics can be relieved and the intensities of absorption peaks of Er^{3+} (381, 487, and 524 nm) decrease to some extent. And the absorption peak centered at 225 nm disappears, corresponding to the strengthening of the absorption peak centered at 255 nm.

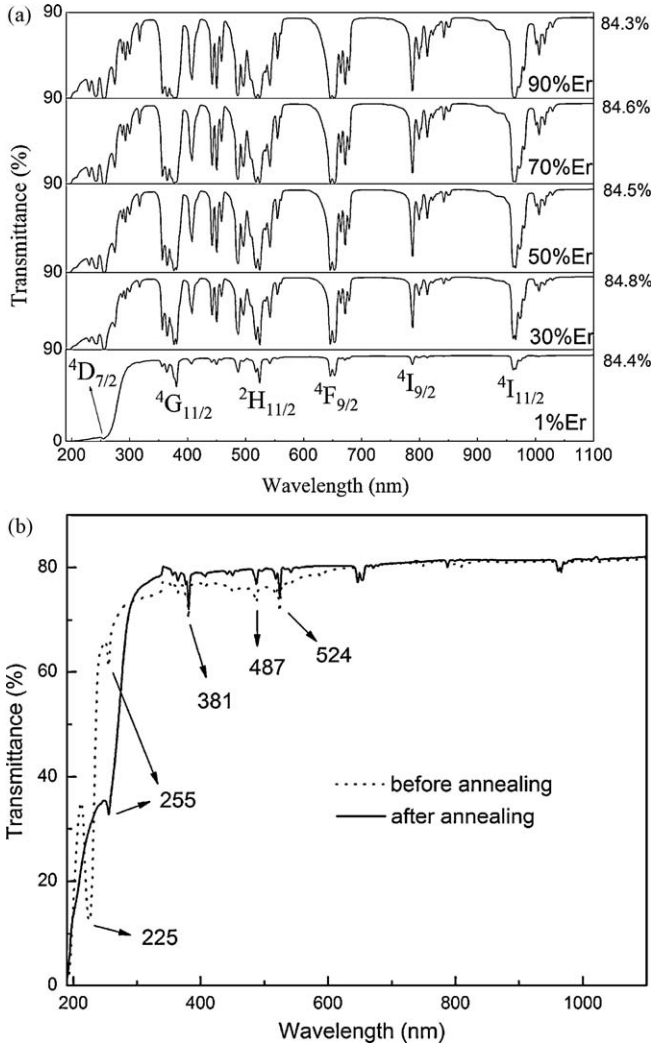

Fig. 2. (a) The in-line transmittance spectra of Er:YAG ceramics with erbium content of 1%, 30%, 50%, 70%, and 90% respectively (thickness = 2 mm); (b) the in-line transmittance spectra of 0.5%Er:YAG ceramics before and after air annealing (thickness = 2 mm).

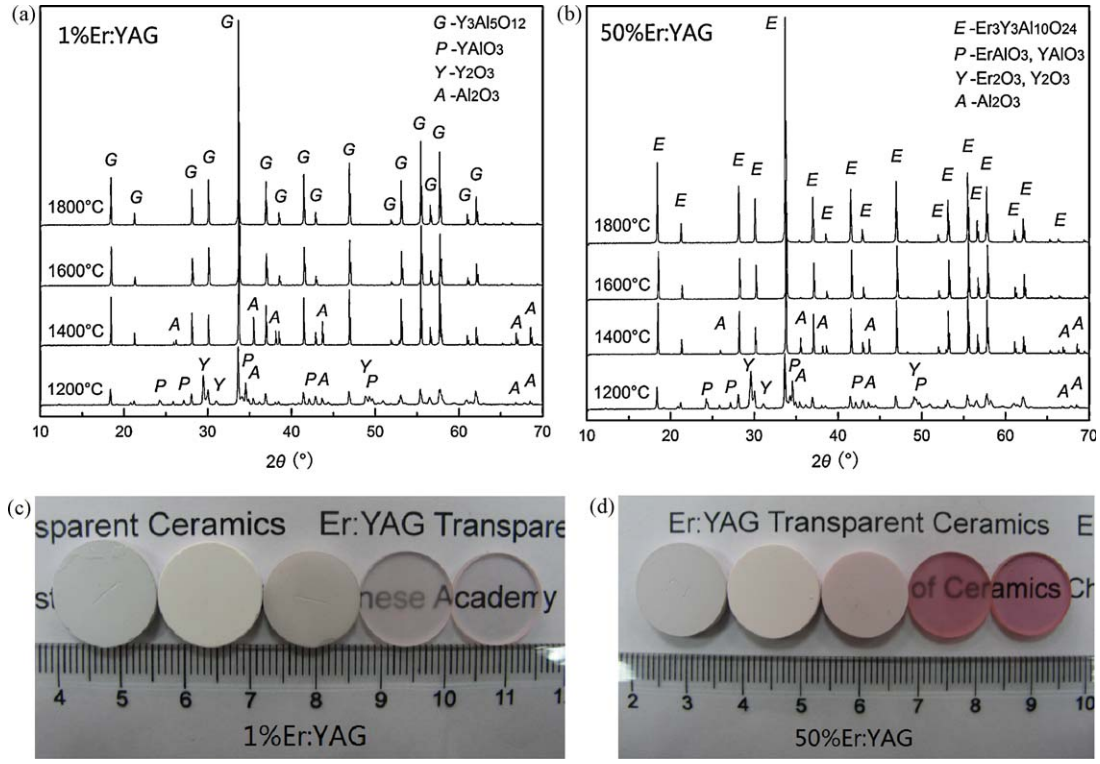

Fig. 3. (a, b) The XRD patterns of 1%Er:YAG and 50%Er:YAG ceramics vacuum-sintered at different temperature for 2 h; (c, d) the photographs of the 1%Er:YAG and 50%Er:YAG ceramics.

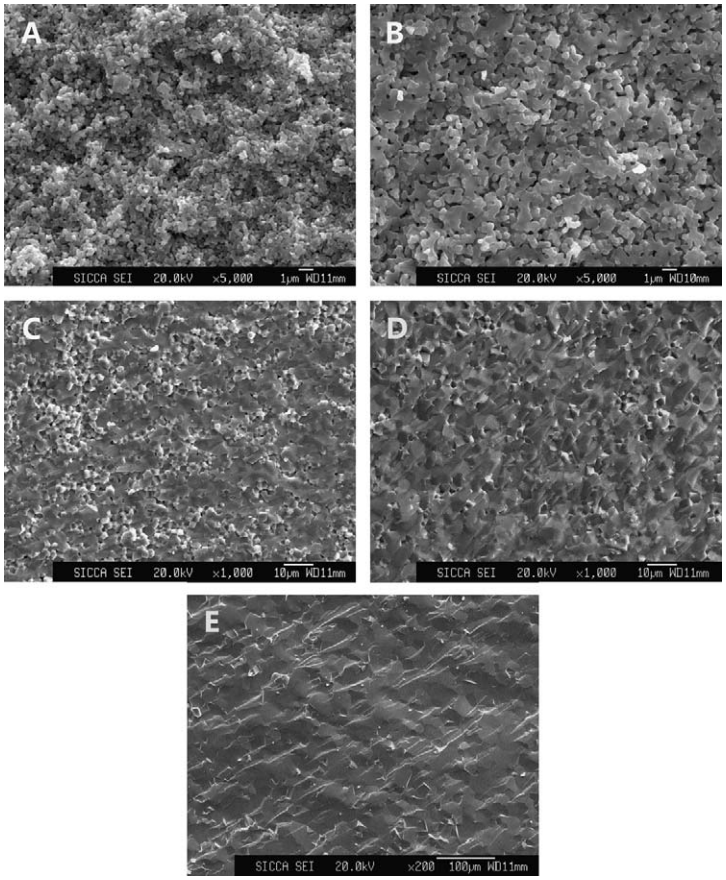

Fig. 4. The fracture microstructures of the 1%Er:YAG ceramics (from A to E: 1200 °C × 2 h, 1400 °C × 2 h, 1600 °C × 2 h, 1800 °C × 2 h and 1800 °C × 30 h).

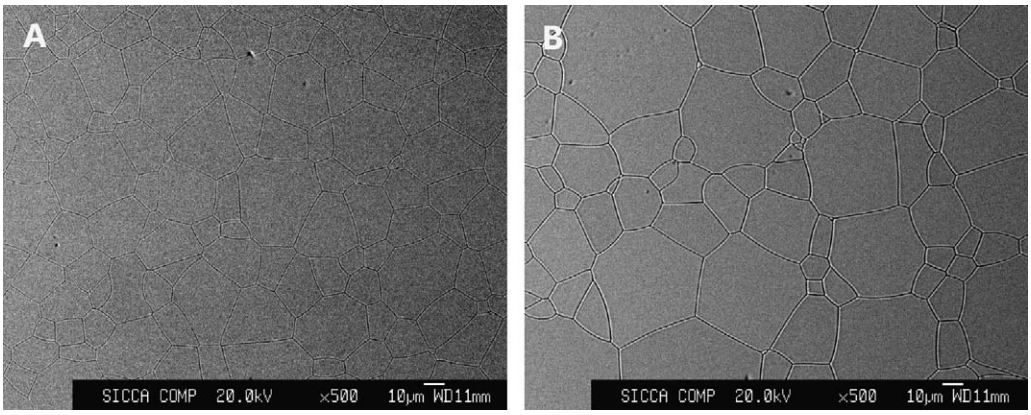

Fig. 5. The EPMA photographs of the 1%Er:YAG (A) and 90%Er:YAG (B) ceramics.

Fig. 3(a) and (b) respectively show the XRD patterns of 1%Er:YAG and 50%Er:YAG ceramics vacuum-sintered at different temperatures for 2 h. For 1%Er:YAG ceramics, the YAG phase can be observed along with residual YAP ($YAlO_3$) phase at 1200 °C. While the temperature increases, more and more aluminum atoms turn into parts of YAG grains. Al_2O_3 particles do not exist above 1600 °C, and the phase transformation terminates. It can be seen from Fig. 3(b) that the phase transformation of 50%Er:YAG is just similar with that of 1%Er:YAG, and the phase $Er_3Y_3Al_{10}O_{24}$ is finally obtained. The different contents of erbium element do not affect the phase transformation temperature significantly, and the best sintering temperatures of all studied ceramics are all about 1800 °C. Fig. 3(c) and (d) are photographs of the 1%Er:YAG and 50%Er:YAG ceramics respectively. From left to right, the sintering processes are 1200 °C × 2 h, 1400 °C × 2 h, 1600 °C × 2 h, 1800 °C × 2 h and 1800 °C × 30 h respectively, and the last two samples have been mirror-polished. After vacuum-sintered at about 1800 °C, the ceramics achieve a high density and begin to getting transparent along with the pores reducing and disappearing. In order to get the best transparency, enough long soaking time is necessary. The

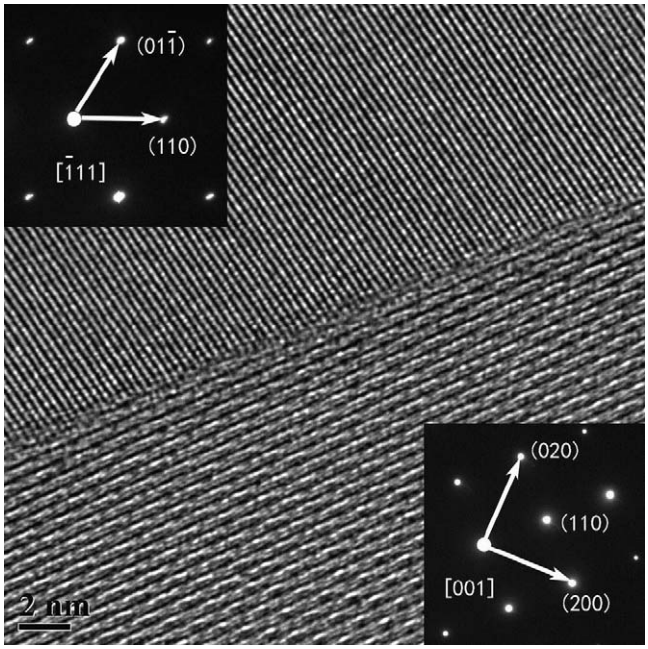

Fig. 6. The HRTEM photograph of grain boundary from the 1%Er:YAG ceramics.

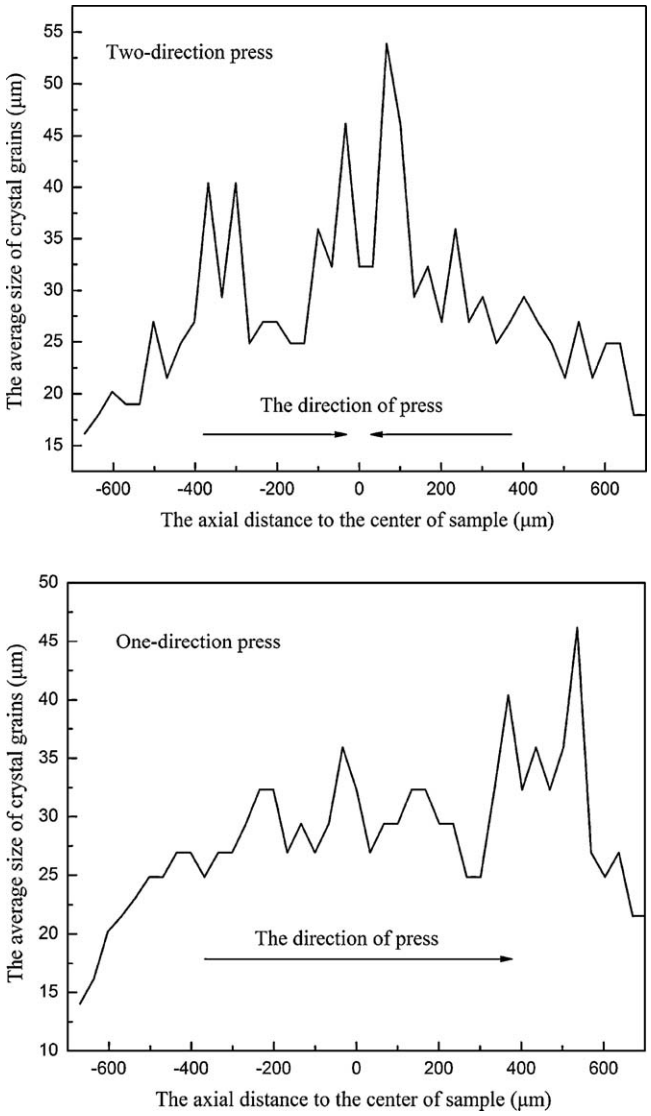

Fig. 7. The dependence of grain sizes on the axial distance to the center of samples using one-direction press and two-direction press respectively.

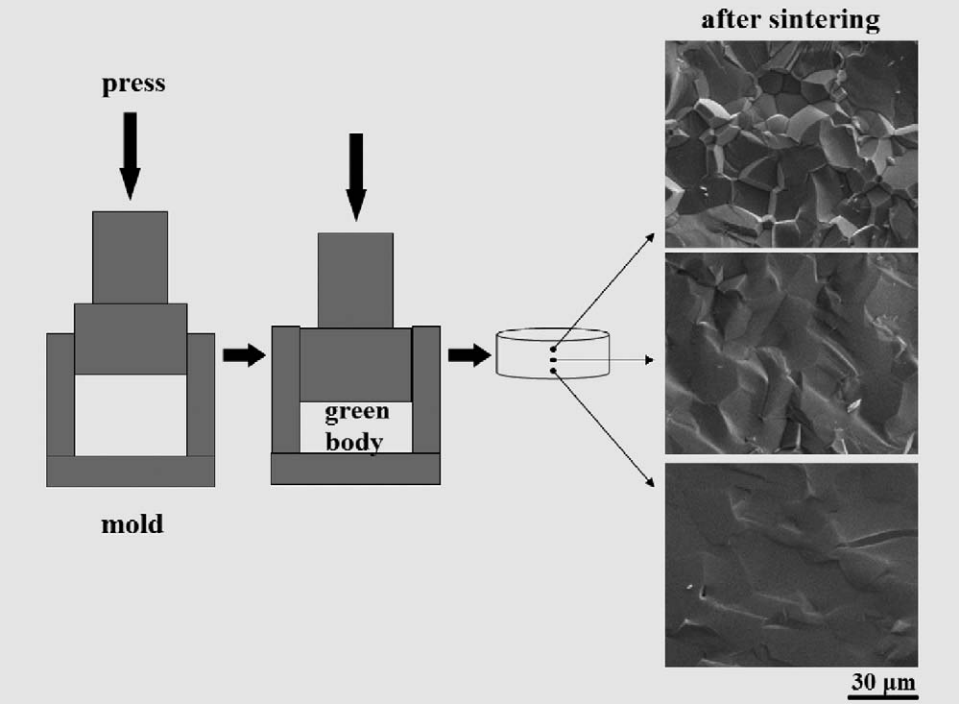

Fig. 8. The scheme of the relationships between one-direction press and grain sizes distribution.

fracture microstructures of these ceramics are shown in Fig. 4. We can see that main densification process occurs during the sintering procedure from 1400 to 1600 °C. In this temperature section, crystal nucleuses begin to emerge and fast multiply. After sintered at 1600 °C for 2 h, most of the grains contact closely and the sizes of the grains are about 2–3 μm. And intercrystalline fracture is the main fracture model. With the sintering temperature and soaking time increasing, more and more grains start uniting and keep growing up, corresponding to more and more transgranular fracture.

According to the EPMA photographs shown in Fig. 5, it is found that the samples are very compact with very few pores. There are no secondary phases observed both at the grain boundaries and the inner grains. The average grain size of the 1%Er:YAG ceramics is about 30 μm. Due to the large particle size of starting powder Er_2O_3, the average grain size of the 90%Er:YAG ceramics is obviously larger than that of the 1%Er:YAG ceramics. The high-resolution TEM micrograph (HRTEM) of the grain boundary in the 1%Er:YAG ceramics is shown in Fig. 6. The grain boundary is clean and narrow with a width of about 1 nm, so the optical scattering caused by boundaries will be insignificant. The insets in Fig. 6 are the corresponding electron diffraction patterns of the grains on the both sides of the boundary. It can be seen that both grains are

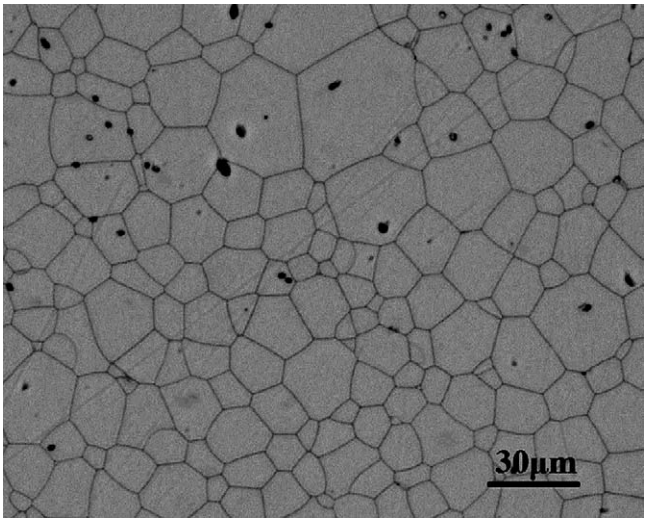

Fig. 9. The microstructure of cross section from the 1%Er:YAG ceramics.

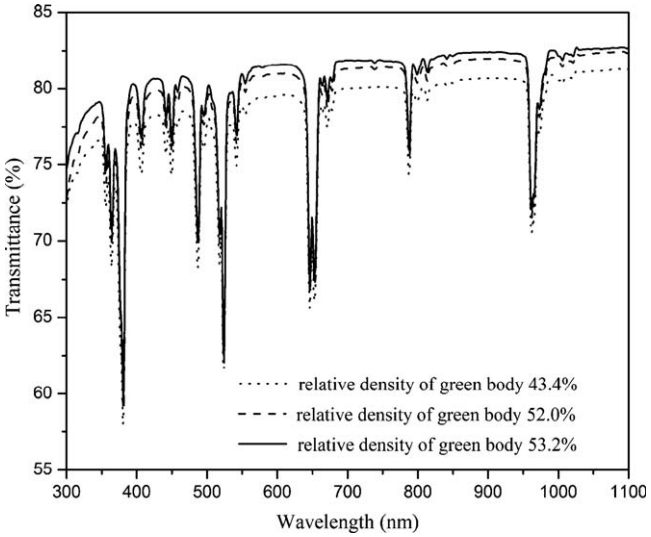

Fig. 10. The transmittance spectra of mirror-polished 1%Er:YAG ceramics (thickness = 2 mm) with different average densities of green bodies.

the same cubic phase with different orientation ([$\bar{1}$ 1 1] and [0 0 1] respectively).

Fig. 7(a) and (b) include two curves respectively representing the grain sizes dependent on the axial distance to the central point of the cylinder sample, which maybe can reflect the relationships between density distribution in green body and microstructure of samples. The average grain sizes were observed by EPMA. It can be found in Fig. 2(a) and (b) that this two curves show quite different trends according to different press way of green body. And we know the main difference between one-direction press and two-direction press is the density distribution in the green body. In this study, the follow-up cold isostatic pressing introduced isostatically press around the green body and only increased total average relative density of the green body a little (<10%), so it cannot change the density distribution significantly. While using two-direction press, the middle part of the green body is possessed of the lowest density, and shows the largest grains after sintering. While using one-direction press, the part with the lowest density is near bottom part of the green body, and shows the largest grains after sintering. And the part with highest density in green body has finest grains after sintering. Therefore it can be probably revealed that high density in green body conduces to fine crystal grains after sintering. The simple scheme is shown in Fig. 8 in the case of one-direction press. It is very difficult to obtain a green body with homogeneous density distribution through dry pressing. Slip casting could be an excellent option to fabricate homogeneous green bodies. Russian researchers have developed a novel high-pressure colloidal slip-casting (HPCSC) method to fabricate Nd:YAG ceramics [18], which may be a significant way to gain homogeneous density distribution in the green body.

As we know, sintering is a shrinkage procedure along with the emergence and growth of crystal grains. When the grains meet each other, the growth is stopped temporarily before the grains merge into large ones and the sample become very compact with almost theoretical density if the grains do not enclose any pores within them. Therefore if grains merging do not happen, when some parts of the green body have higher density, there will be much more grains emerging out and the grains meet each other earlier, so the grain sizes will be smaller. When the grains become larger, it will increase the chance of enclosing pores within them. As shown in Fig. 9, grains are much larger in the upper part of the figure than that in the lower part, and much more pores existing in the upper part than that in the lower part.

Fig. 10 shows the dependence of transparency on average relative density of a whole green body. It is clear that fine densification of green body will lead to excellent transparency. In sintering procedure, the green body with higher density will achieve fully compactness earlier, smaller average grain sizes obtained and less pores remaining in crystal grains as light scattering sources. Therefore to increase the density of green body is a significant way to improve the optics quality of Er:YAG ceramics. Though the study focuses on Er:YAG, the result can be broadly applied to all RE-doped YAG ceramics and other ceramics optical materials.

The luminescence spectra of the Er:YAG ceramics pumped by 980 nm laser diode are shown in Fig. 11. From the energy

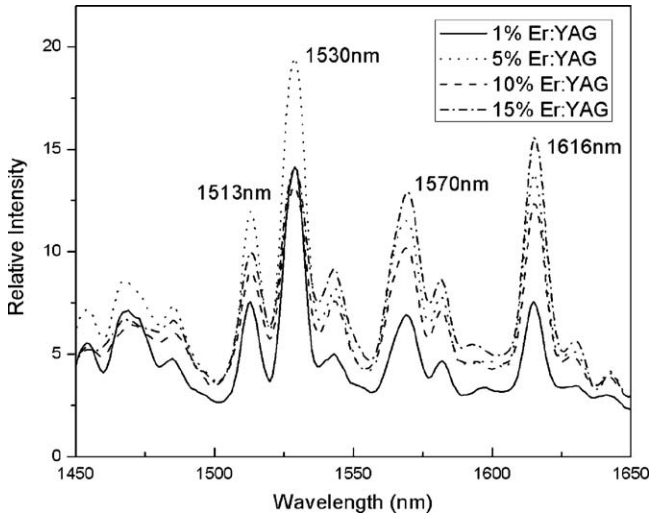

Fig. 11. The fluorescence spectra of the Er:YAG ceramics pumped by a 980 nm LD.

level transition of $^4I_{13/2} \rightarrow {}^4I_{15/2}$, Er^{3+} ions can emit large band of lights from 1450 to 1650 nm wavelength because of spark energy level splitting. The main peaks are centered at 1513, 1530, 1570, and 1616 nm wavelength respectively. When Er^{3+} ion content exceeds 5%, luminescence quenching begins to emerge at 1530 nm wavelength. For 5%Er:YAG ceramics, the luminescence of 1530 nm wavelength is obviously dominant in the band and can be chosen as the aim of laser experiments potentially [19].

4. Conclusions

In this study, highly transparent polycrystalline Er:YAG ceramics with different Er content from 1% to 90% had been obtained by the solid-state reaction and the vacuum-sintering technique. The in-line transmittances of mirror-polished Er:YAG ceramics are all up to 84% at 1100 nm wavelength. All the samples are very compact with very few pores. There are no secondary phases observed both at the grain boundaries and the inner grains. The average grain size of the 1%Er:YAG ceramics is about 30 μm. The grain boundary is clean and narrow with a width of about 1 nm. The best sintering temperatures of all studied ceramics are about 1800 °C. It was found that the parts of green body with highest density correspond to finest grains after sintering. And increasing the density of green body could be a significant way to control the grain sizes in the solid-state reaction and the vacuum-sintering technology. When Er^{3+} ion content exceeds 5%, luminescence quenching begins to emerge at 1530 nm wavelength. For 5%Er:YAG ceramics, the luminescence of 1530 nm wavelength is obviously dominant in the band and can be chosen as the aim of laser experiments potentially.

Acknowledgements

This work was supported by Chinese National Science Foundation (No. 50990300), the 863 project (No. AA03Z523), the Natural Science Foundation of Shanghai (No. 10ZR1433900), and the Major Basic Research Programs of

Shanghai (No. 07DJ14001). And I really appreciate the encouragement and great help from Academician of CAS, Prof. Jing-kun Guo and Prof. Li-ping Huang.

References

[1] A. Ikesue, T. Kinoshita, K. Kamata, K. Yoshida, Fabrication and optical properties of high-performance polycrystalline Nd:YAG ceramics for solid-state lasers, J. Am. Ceram. Soc. 78 (4) (1995) 1033–1040.
[2] T. Yanagitani, H. Yagi, M. Ichikawa, Japanese patent 10-101333 (1998).
[3] J. Lu, M. Prabhu, J. Xu, K. Ueda, H. Yagi, T. Yanagitani, A.A. Kaminskii, Highly efficient 2% Nd:yttrium aluminum garnet ceramic laser, Appl. Phys. Lett. 77 (23) (2000) 3707–3709.
[4] J. Lu, T. Murai, K. Takaichi, T. Uematsu, K. Misiwa, M. Prabhu, J. Xu, K. Ueda, H. Yagi, T. Yanagitani, A.A. Kaminskii, 72 W Nd:$Y_3Al_5O_{12}$ ceramic laser, Appl. Phys. Lett. 78 (23) (2001) 3586–3588.
[5] J. Lu, H. Yagi, K. Takaichi, T. Uematsu, J. Bisson, Y. Feng, A. Shirakawa, K. Ueda, T. Yanagitani, A.A. Kaminskii, 110 W ceramic Nd^{3+}:$Y_3Al_5O_{12}$ laser, Appl. Phys. B 79 (2004) 25–28.
[6] A. Ikesue, Y.L. Aung, T. Taira, T. Kamimura, K. Yoshida, G.L. Messing, Progress in ceramic lasers, Annu. Rev. Mater. Res. 36 (2006) 397–429.
[7] A. Ikesue, Y.L. Aung, T. Yoda, S. Nakayama, T. Kamimura, Fabrication and laser performance of polycrystal and single crystal Nd:YAG by advanced ceramic processing, Opt. Mater. 29 (2007) 1289–1294.
[8] H. Yagi, T. Yanagitani, K. Takaichi, K. Ueda, A.A. Kaminskii, Characterizations and laser performances of highly transparent Nd^{3+}:$Y_3Al_5O_{12}$ laser ceramics, Opt. Mater. 29 (2007) 1258–1262.
[9] Y. Wu, J. Li, Y. Pan, Q. Liu, J. Guo, B. Jiang, J. Xu, Diode-pumped passively Q-switched Nd:YAG ceramic laser with a Cr:YAG crystal saturable absorber, J. Am. Ceram. Soc. 90 (5) (2007) 1629–1631.
[10] Y. Wu, J. Li, Y. Pan, J. Guo, B. Jiang, Y. Xu, J. Xu, Diode pumped Yb:YAG ceramic laser, J. Am. Ceram. Soc. 90 (10) (2007) 3334–3337.
[11] J. Li, Y. Wu, Y. Pan, W. Liu, L. Huang, J. Guo, Fabrication, microstructure and properties of highly transparent Nd-YAG laser ceramics, Opt. Mater. 31 (1) (2008) 6–17.
[12] J. Li, Y. Wu, Y. Pan, W. Liu, L. Huang, J. Guo, Laminar structured YAG/Nd:YAG/YAG transparent ceramics for solid-state lasers, Int. J. Appl. Ceram. Technol. 5 (4) (2008) 360–364.
[13] D. Chen, C.L. Fincher, T.S. Rose, F.L. Vernon, R.A. Fields, Diode-pumped 1-W continuous-wave Er:YAG 3-μm laser, Opt. Lett. 24 (6) (1999) 385–387.
[14] R. Hibst, U. Keller, Experimental studies of the application of the Er:YAG laser on dental hard substances: I. Measurement of the ablation rate, Lasers Surg. Med. 9 (4) (2005) 338–344.
[15] A. Ikesue, K. Yoshida, T. Yamamoto, I. Yamaga, Optical scattering centers in polycrystalline Nd:YAG laser, J. Am. Ceram. Soc. 80 (6) (1997) 1517–1522.
[16] M.O. Ramirez, J. Wisdom, H. Li, Y.L. Aung, J. Stitt, G.L. Messing, V. Dierolf, Z. Liu, A. Ikesue, R.L. Byer, V. Gopalan, Three-dimensional grain boundary spectroscopy in transparent high power ceramic laser materials, Opt. Express 16 (9) (2008) 5965–5973.
[17] X. Zeng, G. Zhao, J. Xu, H. Li, X. He, H. Pang, M. Jie, Effect of air annealing on the spectral properties of Ce:$Y_3Al_5O_{12}$ single crystals grown by the temperature gradient technique, J. Cryst. Growth 274 (2005) 495–499.
[18] Yu.L. Kopylov, V.B. Kravchenko, S.N. Bagayev, V.V. Shemet, A.A. Komarov, O.V. Karban, A.A. Kaminskii, Development of Nd^{3+}:$Y_3Al_5O_{12}$ laser ceramics by high-pressure colloidal slip-casting (HPCSC) method, Opt. Mater. 31 (2009) 707–710.
[19] A.A. Kaminskii, Laser crystals and ceramics: recent advances, Laser Photonics Rev. 2 (2007) 93–177.